metals

MDPI

Article

The Influence of Multiple Pass Submerged Friction Stir Processing on the Microstructure and Mechanical Properties of the FSWed AA6082-AA8011 Joints

Sipokazi Mabuwa * and Velaphi Msomi

Mechanical Engineering Department, Cape Peninsula University of Technology, Bellville 7535, South Africa; msomiv@gmail.com

* Correspondence: sipokazimabuwa@gmail.com; Tel.: +27-21-953-8778

Received: 28 September 2020; Accepted: 19 October 2020; Published: 28 October 2020

Abstract: The AA6082–AA8011 friction stir-welded joints were subjected to submerged multiple pass friction stir processing to evaluate the microstructure and mechanical properties of the joints. A maximum of four submerged friction stir processed passes were used in this study. All the specimens were extracted from three different joint positions (start, middle and end). The tests conducted included microstructural analysis, tensile tests, hardness and fracture surface morphology of the post-tensile specimens, were performed using a scanning electron microscope (SEM). There was no particular trend in the microstructure and mechanical properties when looking at the specimen positioning in all the passes. The minimum mean grain sizes were refined from 3.54 to 1.49 µm and the standard deviation from 5.43 to 1.87 µm. The ultimate tensile strength was improved from 84.96 to 94.77 MPa. The four-pass SFSPed specimens were found to have more ductile properties compared to the one-pass SFSPed one. The hardness of the stir zones in all the passes was found to be higher compared to the AA8011 base material but lower than the AA6082 one. The maximum stir zone hardness of 75 HV was observed on the one-pass SFSP joints.

Keywords: microstructure; submerged friction stir processing; dynamic recrystallization; tensile properties; hardness; fracture surface morphology

1. Introduction

Friction stir processing (FSP) is an advanced microstructural altering process based on the friction stir welding process [1,2]. The grain refinement is a result of the dynamic recrystallization that occurs during the process. The FSP technique does not only refine the microstructural grain size but also modifies the texture of the processed zone [3,4]. FSP has been successfully used in many applications including the fabrication of surface composites of aluminium substrates [5,6], for superplastic high strain rate [7,8], metal matrix composites [9,10] and cast aluminium alloys [11,12]. FSP as an enticing emerging technology continues to grow, however, due to the high temperature the material experiences during FSP, grain growth was found to occur. Submerged friction stir processing (SFSP) came as a solution to minimize grain growth in order to achieve more grain refinement [13]. The SFSP technique works similarly to the normal or rather traditional FSP, the only difference takes place under controlled immersed environments [14,15].

Several studies have investigated the effect of submerged friction stir processing on aluminium alloys. Feng et al. [16] evaluated the impact of submerged friction stir processing on the microstructure of the AA2219–T6 plate. The processing conditions included the traverse speed of 200 mm/min and varying rotational speed. The results showed that the hardness of the stir zone was found to decrease with an increase in rotational speed. The decrease was substantiated to be due to softening of the

processed zone resulting from precipitate hardening. The average grain size was found to be finer than the base material one. The AA6082/AA8011 dissimilar friction stir-welded joint was subjected to SFSP to investigate the changes in the microstructure and mechanical properties of the joints [17]. The results revealed that the average grain size decreased in comparison to that of the friction stir welded and base material one. The tensile strength and the hardness of the submerged processed joints were reported to increase in comparison to that of the friction stir-welded one. Patel et al. [18] proved that FSP active cooling methods in the form of compressed air, water and carbon dioxide (CO_2) can enhance the superplastic behaviour of the high strength AA7075 alloy. Amongst the cooling methods used, the CO_2 produced the lowest temperature readings due to higher cooling rate, resulting in the prevention of the coarsened grains in the stir zone. This, therefore, resulted in the CO_2 having very fine grain sizes compared to other cooling methods. However, all the cooling methods were found to have finer grains compared to the normal friction stir-processed ones. Similar studies where the application of SFSP resulted in finer microstructural grain size were reported [19–22].

A few studies where the SFSP underwent multiple passes were found in the literature. Srivastava et al. [23] investigated the influence of the multiple passes on the microstructure and mechanical properties of the AA5059/SiC surface composites fabricated via submerged friction stir processing. The results revealed an increase from 85 to 159 HV in the hardness of the four-pass SFSPed specimen in comparison to the hardness value of the base material. The ultimate tensile strength (UTS) was also found to increase in the four-pass specimen from 321 MPa of the base material one to a 377 MPa. Additionally, the SFSPed UTS was also higher compared to the that of four-pass FSP under normal conditions, which was 347 MPa. The grain sizes were also noted to be finer on the SFSPed specimens compared to the normal friction stir-processed specimens. Huang et al. [24] subjected the AA5083/TiC to multiple pass SFSP to form bulk aluminium matrix composites. It was reported that the addition of water cooling resulted in a strong suppression of effect on the growth of the recrystal grain, while the addition of the TiC particles boosted recrystallization, owing to the extra dislocations generated at Ti/Al. The formation of the aluminium matrix composites (AMCs) resulted in the microstructural average grain size of about 1 µm. The yield strength and the UTS improved from 78 to 153 MPa in comparison to the base material. The fracture surface morphology of the SFSPed AMCs showed ductile behaviour represented by the well developed small uniform dimples. Similar studies where the multiple pass SFSP resulted in finer grain sizes and improved mechanical properties were reported in the literature [25–27].

It has been noted that most of the available work on the multiple pass SFSP of aluminium alloys is on the surface composites. The available literature also reports on the multiple pass SFSP of the single surface, but there is no searchable work where multiple passes were applied on the welded joints. This study investigates the influence of the multiple pass SFSP on the microstructure and mechanical properties of the friction stir-welded dissimilar aluminium alloys of AA6082-AA8011 joints.

2. Materials and Methods

Aluminium alloy AA6082–T651 and AA8011–H14 were used in this study. The chemical compositions of the materials are shown in Table 1. The dissimilar aluminium alloys were cut into dimensions of 6 mm × 250 mm × 55 mm. A total number of 4 pairs were friction stir welded, positioning the AA6082 alloy on the advancing side and the AA8011 alloy on the retreating side. The semi-automated Lagun FA.1 milling machine was used for the friction stir welding (FSW) process. The process parameters used for FSW are shown in Table 2. A triangular threaded tool made of high-speed steel (HSS) AISI 4140 was used for both FSW. Figure 1a shows the friction stir welding setup. Table 3 shows the grain size and mechanical properties of the base materials and FSW joint. The friction stir-welded joints were then friction stir processed underwater (submerged) using the same parameters used for FSW. The first plate was processed with a one-pass (1-pass), the second one with a two-pass (2-pass), the third one with a three-pass (3-pass) and the fourth one with a four-pass FSP. Figure 1b shows SFSP setup, highlighting that the one-pass SFSP and the four-pass (4-pass) SFSP

shown in Figure 1c were applied to the FSW joint. The same tool and parameters used for friction stir welding were also used for friction stir processing.

Table 1. Chemical compositions [28,29].

	Mg	Ti	Zn	Cr	Si	Mn	Fe	Cu	Al
AA8011–H14	0.28	0.016	0.084	0.028	0.52	0.46	0.74	0.13	Bal
AA6082–T651	0.6–1.2	-	0.0–0.1	0.0–0.25	0.7–1.3	0.4–1.0	0.0–0.5	0.0–0.1	Bal

Table 2. Friction stir welding and submerged friction stir processing process parameters.

Tool Traverse Speed (mm/min)	Tool Rotation Speed (rpm)	Tool Tilt Angle (°)	Tool Pin Diameter (mm)	Tool Shoulder (mm)	Tool Pin Length (mm)
55	1200	2	7	20	5.8

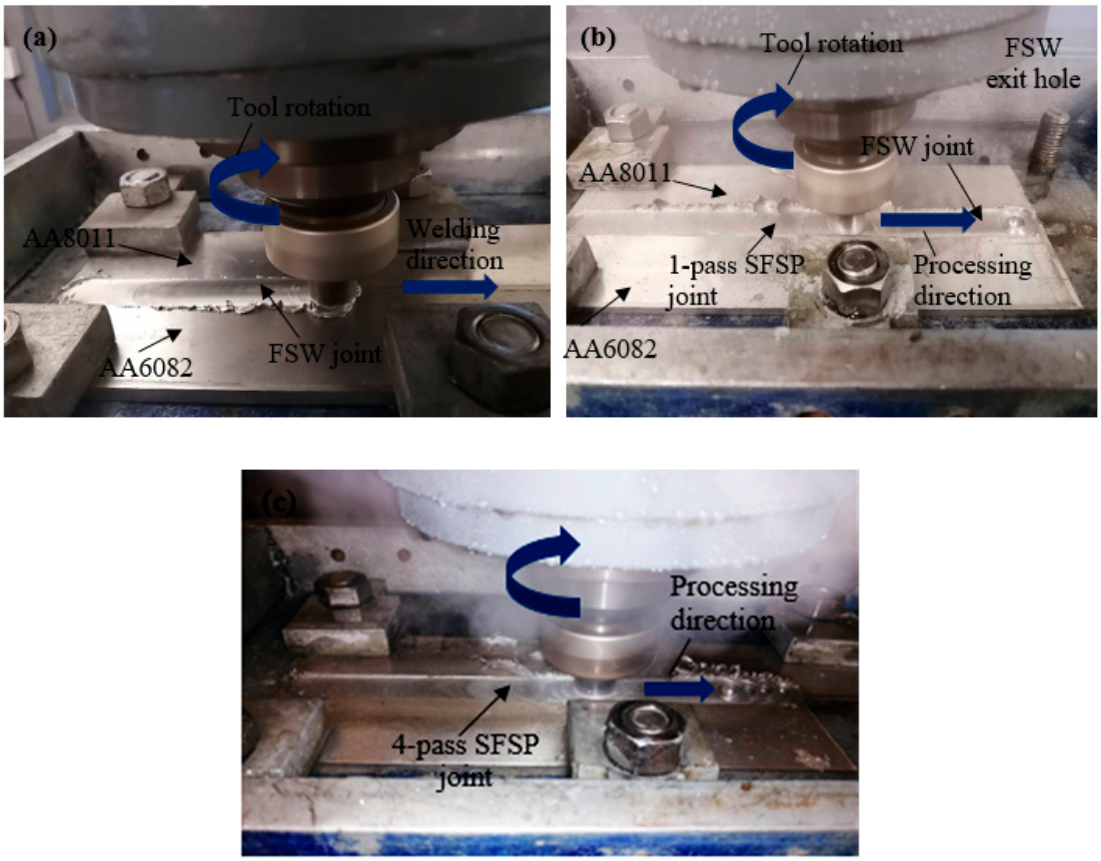

Figure 1. (**a**) Friction stir welding process, (**b**) one-pass submerged friction stir processing (SFSP) and (**c**) four-pass SFSP.

Table 3. Grain size and mechanical properties of the base materials and FSW joint [17,30].

	Average Grain Size (μm)	Ultimate Tensile Strength (MPa)	Average Elongation (%)	Microhardness (HV)
AA8011–H14	51.57	94.1	40.17	33.8
AA6082–T651	65.04	308	25.42	92
FSW AA6082–AA8011	16.77 (stir zone)	82.9	17.98	58 (stir zone)

The friction stir-processed plates (FSPed) were cut for different tests using waterjet cutting technology. The tests conducted were the tensile test, microhardness, microstructural analysis and fatigue test. The Hounsfield 50 K tensile testing machine was used to perform the tensile tests of

the specimens. The tensile specimen geometry and operating parameters were adapted from the ASTM-E8M-04 standard. Figure 2a depicts the tensile test specimen used in this study. The fractured tensile specimens were further analysed for the nature of fracture and morphology using a Tescan MIRA3 RISE scanning electron microscope (TESCAN Orsay Holding, Kohoutovice, Czech Republic). The InnovaTest Falcon 500 hardness testing machine (INNOVATEST Europe BV Manufacturing, Maastricht, The Netherlands) was used to perform the Vickers hardness test following the ASTM E384-11 standard. Figure 2b presents the specimen used for microhardness testing. The objective 10× and objective 20× for specimen focusing were used during setup. A 0.5 kg load and 1 mm interval was applied from the centre to either side of the specimen (advancing and retreating). A single line pattern was used to perform the hardness tests.

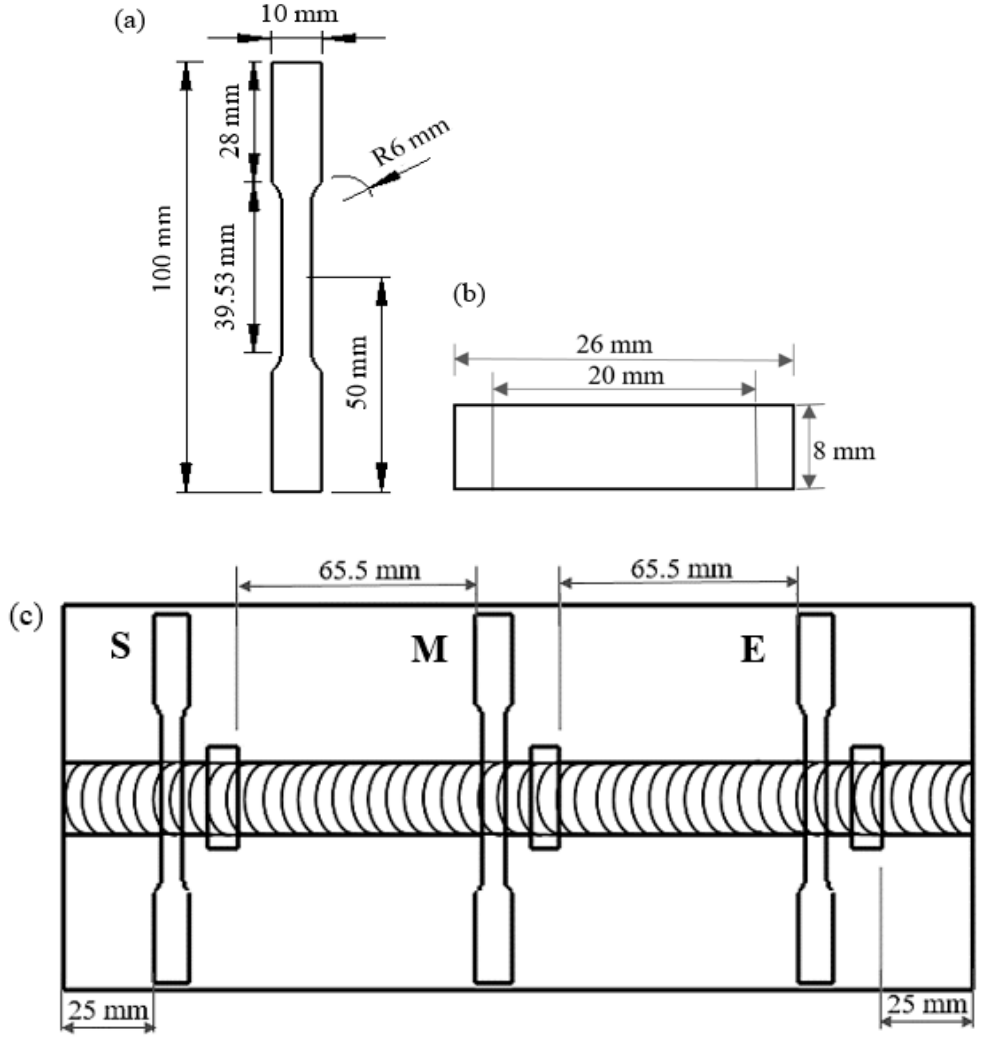

Figure 2. (**a**) Tensile specimen, (**b**) hardness and microstructure specimen, (**c**) specimen positioning diagram.

The microstructural analysis was performed using the Motic AE2000 metallurgical microscope (Motic Europe S.L.U., Barcelona, Spain). The specimens were mounted, ground, polished and etched using the modified Keller's and Weck's agents. The modified Keller's reagent chemical composition was 10 mL nitric acid (HNO_3), 1.5 mL hydrochloric acid (HCl), 1.0 mL hydrofluoric acid (HF) and 87.5 mL distilled water (H_2O) and the Weck's reagents composition was 1 g sodium hydroxide (NaOH), 4 g potassium permanganate ($KMnO_4$) and 100 mL distilled water (H_2O). The ASTM E112-12 standard was used to determine average grain size through the use of ImageJ software. Figure 2c shows the specimen positioning used in this study where "S" represents specimens extracted from the start,

"M" is used for specimens extracted from the middle, and "E" for specimens extracted towards the end of the processed area.

3. Results and Discussions

3.1. Microstructural Analysis

Figure 3 shows the microstructural grain sizes of the multiple passes of submerged friction stir-processed FSWed joints. Table 4 presents the grain sizes measured concerning Figure 3. The 1-pass friction stir-processed FSWed joints had a mean grain size range of 13.17 to 16.51 μm, minimum grain size range of 3.29 to 3.63 μm and a standard deviation range of 4.32 to 6.42 μm. Similar results were reported in the literature [17]. The 2-pass friction stir-processed FSWed joints had a mean grain size range of 7.03 to 7.51 μm, standard deviation range of 2.12 to 3.56 μm and minimum grain size of 3.04 to 4.12 μm. The second pass had a mean grain size range of 5.61 to 6.36 μm, a standard deviation range of 2.03 to 2.61 μm and minimum grain size range of 2.54 to 3.36 μm. The fourth pass had a mean grain size range of 5.03 to 5.38 μm, a standard deviation range of 1.65 to 2.18 μm and a minimum grain size ranges of 1.20 to 1.86 μm. The minimum grain size, mean grain size and the standard deviation decreased with an increase in the number of SFSP passes. The mechanism behind the grain refinement is based on the high plastic deformation and repeated dynamic re-crystalization that occurred during the SFSP process. Furthermore, the post-grain growth during the SFSP is also prevented by the removal of excess frictional heat as a result of rapid water cooling.

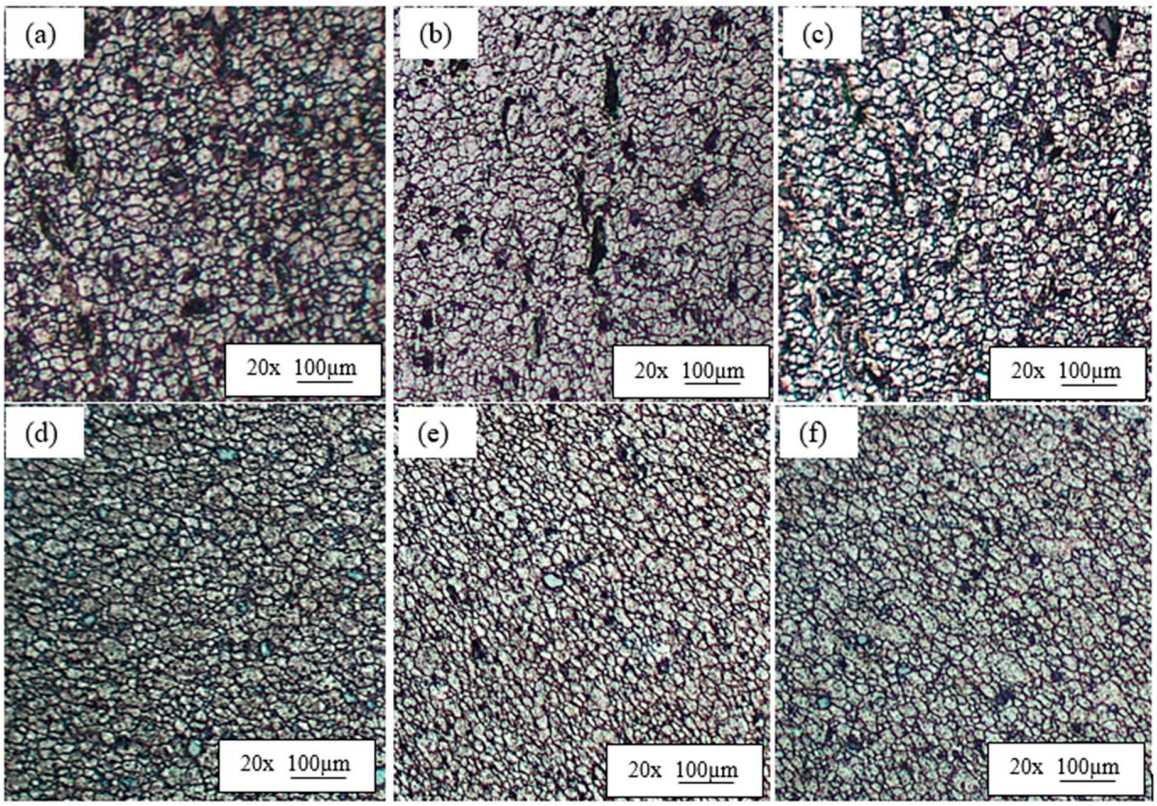

Figure 3. *Cont.*

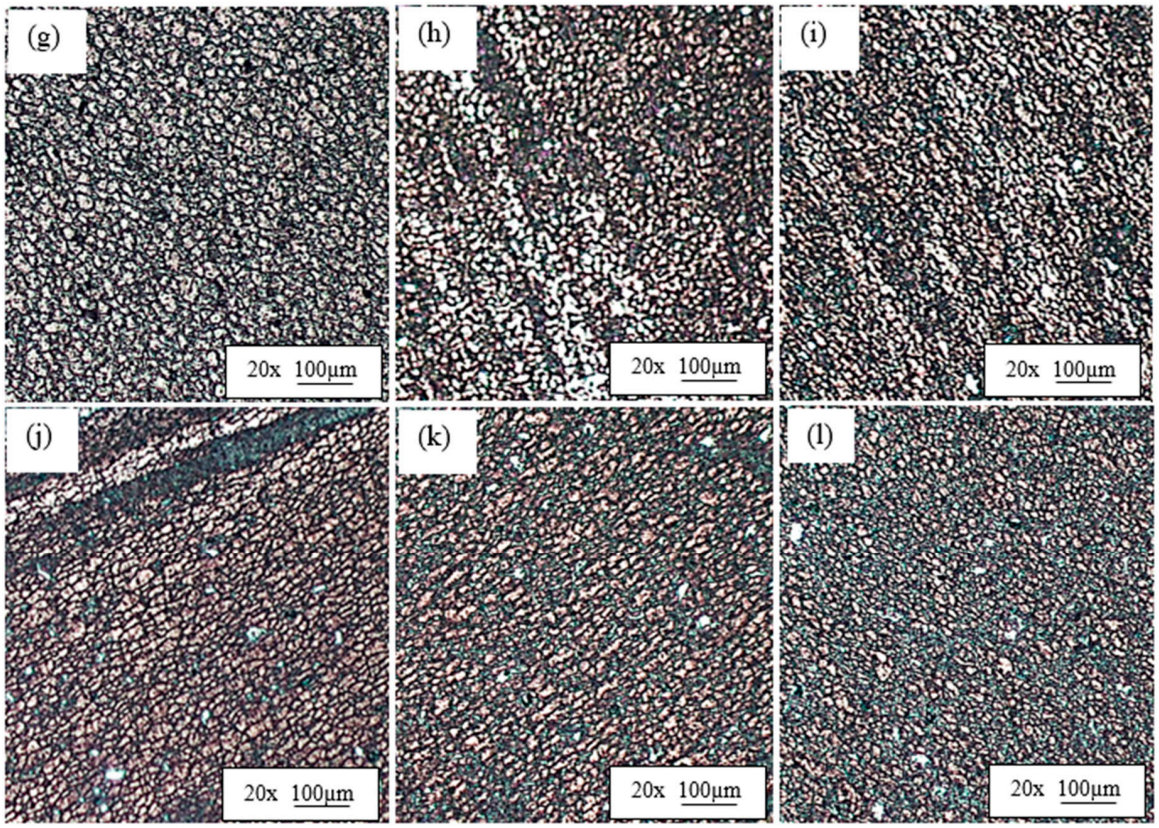

Figure 3. Multiple pass submerged friction stir-processed FSWed micrographs: 1-pass (**a**) start, (**b**) middle, (**c**) end; 2-pass (**d**) start, (**e**) middle, (**f**) end; 3-pass (**g**) start, (**h**) middle, (**i**) end; 4-pass (**j**) start, (**k**) middle, (**l**) end.

Table 4. Measured grain sizes.

No. of SFSP Passes	Specimen Position	Mean Grain Size (μm)	Standard Deviation (μm)	Minimum Mean Grain Size (μm)
1-pass	S	15.69	6.42	3.63
	M	16.51	5.52	3.74
	E	13.17	4.32	3.29
2-pass	S	7.51	3.76	4.04
	M	7.03	3.13	3.04
	E	7.36	3.56	4.12
3-pass	S	5.61	2.12	3.26
	M	6.03	2.03	2.54
	E	6.36	2.61	3.36
4-pass	S	5.15	1.65	1.20
	M	5.03	1.78	1.86
	E	5.38	2.18	1.42

The microstructural grains during the SFSP process reduced the grain growth and the migration rate of grain boundaries, which then led to fine equiaxed grain structure in the stir zone of the joint [31–33]. Additionally, Lou et al. [34] proved that during the multi-pass SFSP, the processed surface undergoes an enhanced cooling rate caused by water, resulting in significantly refined grain sizes. Regarding the specimen positioning, the measured grain sizes had no specific trend. The average grain sizes are depicted in Figure 4. The average minimum grain sizes for the 1-pass SFSPed joint was 3.56 μm, 3.53 μm for the 2-pass, 2.25 μm for the 3-pass and 1.49 μm for the 4-pass joint. The fourth SFSPed

pass resulted in a very fine homogeneous grain structure. Similar work including the application of multiple pass SFSP was reported in the literature [34–36].

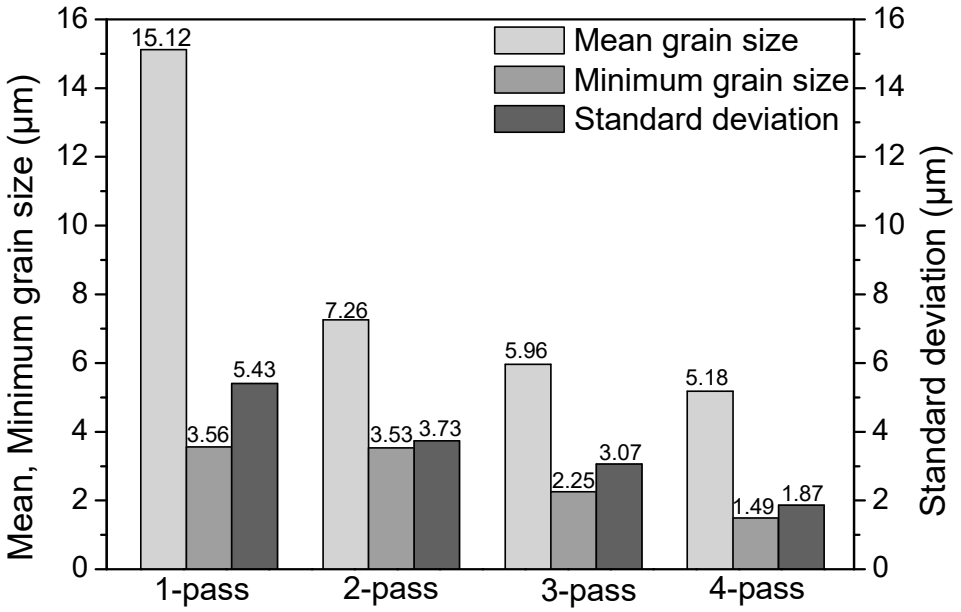

Figure 4. Multiple pass submerged friction stir-processed FSWed average grain sizes.

3.2. Tensile Properties

Figure 5 depicts the tensile stress and strain curves for the multiple submerged friction stir-processed FSWed joints. It is evident that the UTS increased with an increase in the number of SFSP passes. The tensile strain also followed the same trend except for the 2-pass SFSP, which had lower strain compared to the rest of the passes. This was due to the joint having a tunnel defect. Looking at specimen positioning as depicted in Figure 6a, there was no particular trend noticed for the UTS in all the passes, but for the percentage elongation, the 2-pass SFSP one increased towards the specimen extracted toward the end of the joint. Figure 6b shows the average UTS and percentage elongation. Both the average UTS and the percentage elongation increased as the number of passes increased. However, the percentage elongation of the 2-pass strain and percentage elongation was found to be lower compared to the rest of the passes due to the tunnel defect that was observed. The increase in the tensile strength and percentage elongation correlates with the microstructural grain sizes. Similar studies where the application of submerged multiple pass SFSP increased UTS were reported in the literature [23,35–37].

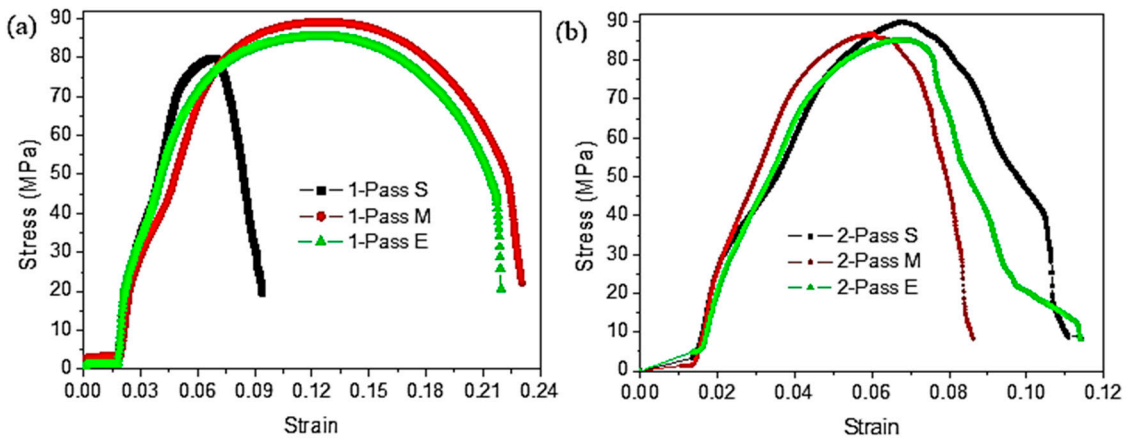

Figure 5. *Cont.*

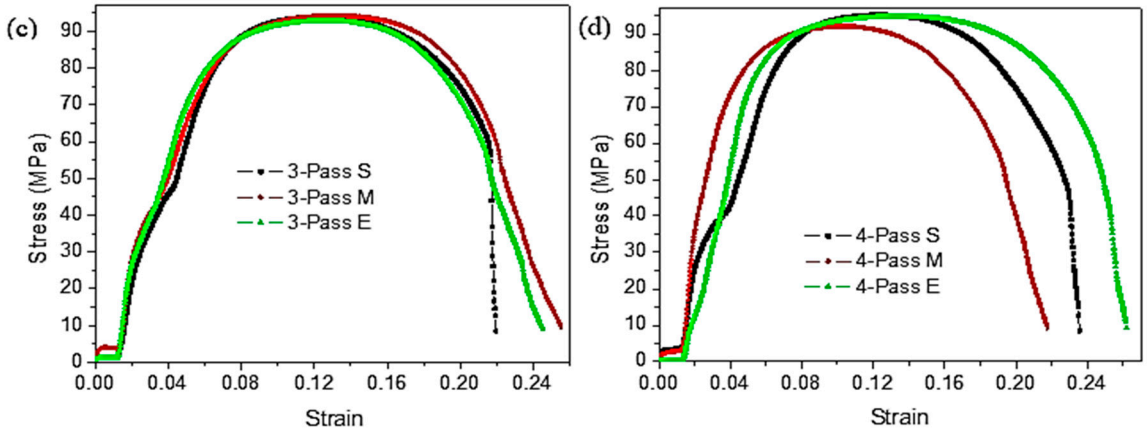

Figure 5. Multiple pass SFSP stress–strain curves, (**a**) 1-pass, (**b**) 2-pass, (**c**) 3-pass and (**d**) 4-pass.

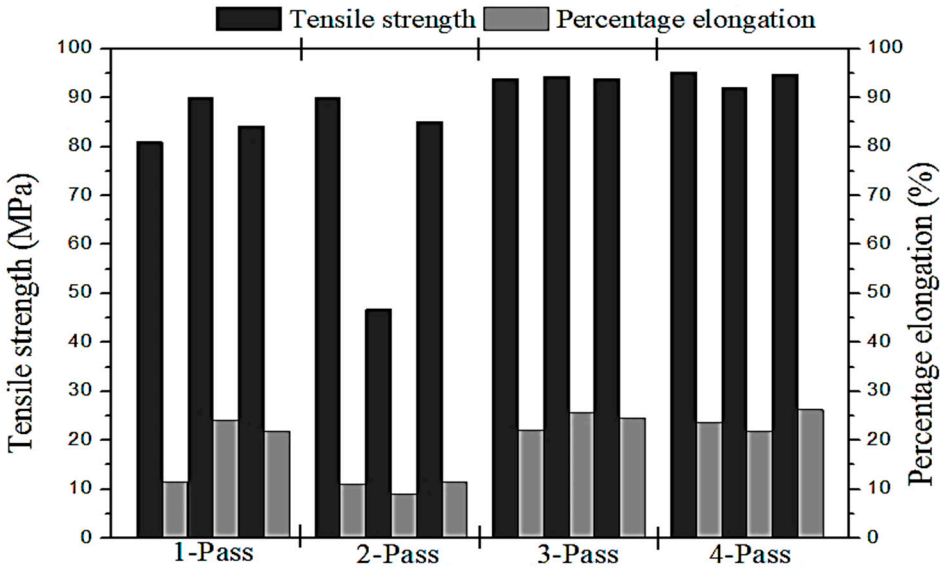

(**a**)

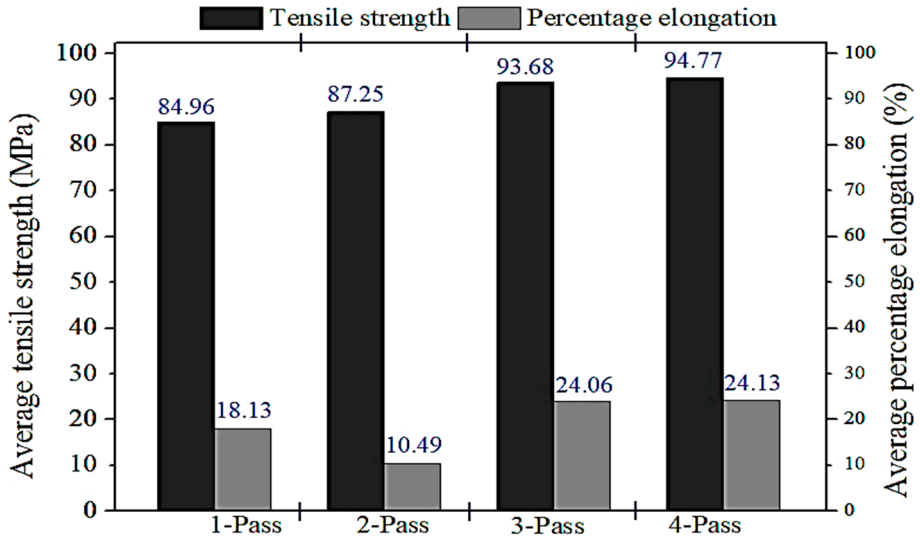

(**b**)

Figure 6. (**a**) Multiple pass SFSP tensile strength and percentage elongation, (**b**) average multiple pass SFSP tensile strength and percentage elongation.

Figure 7 depicts the SEM fracture surface morphologies of the multiple pass SFSPed tensile specimens. All the specimens showed ductile failure with different dimple arrangements. The four-pass showed finer equiaxed dimples compared to the other SFSP passes. The SEM morphologies correlated with the grain sizes of the respective SFSP passes. The morphologies were also in agreement with the percentage elongation results of the specimens [38–40].

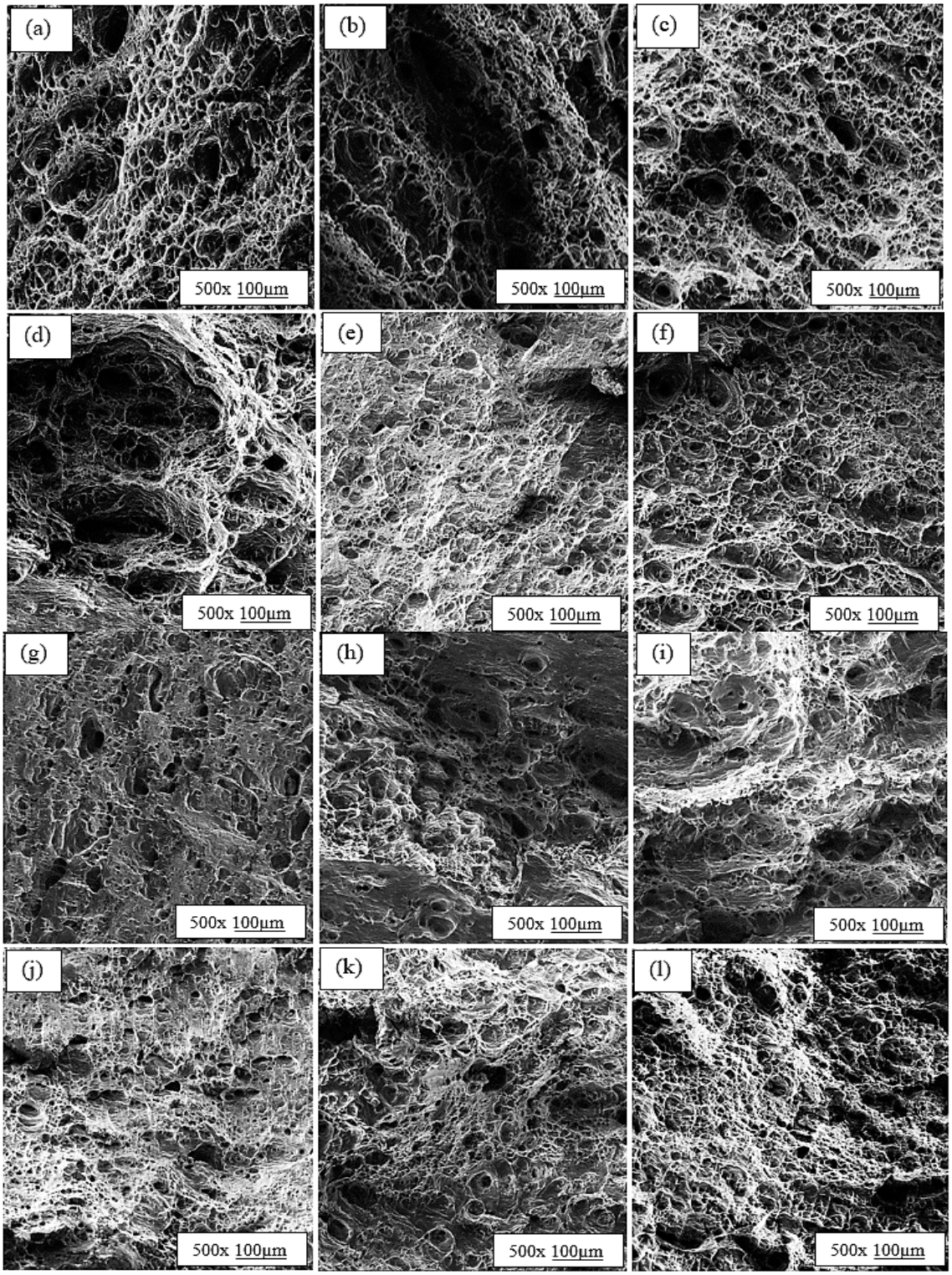

Figure 7. SEM morphologies: 1-pass (**a**) start, (**b**) middle, (**c**) end; 2-pass (**d**) start, (**e**) middle, (**f**) end; 3-pass (**g**) start, (**h**) middle, (**i**) end; 4-pass (**j**) start, (**k**) middle, (**l**) end.

3.3. Hardness

Figure 8 shows the hardness profiles for the multiple pass SFSPed joints. Studying the figure, the specimen extracted in the middle of the joint had higher hardness compared to the specimens extracted towards the start and the end of the joints. Similar observations were noted in the literature [17]. The hardness of the heat-affected zone (HAZ) on the AA6082 side in 1-pass, 3-pass and 4-pass was found to be higher compared to the thermo-mechanical affected zone (TMAZ) and stir zone, while the 2-pass TMAZ hardness was higher compared to the HAZ and stir zone. However, TMAZ, HAZ and stir zone harnesses were lower in all the passes compared to the base material of AA6082. This is due to the AA6082 being precipitate hardened alloy [17,41–43]. The hardness profiles for all the passes declined towards the stir zone and further to the AA8011 side. However, the degree of declining differed according to the number of SFSP passes. Additionally, the hardness of the TMAZ and HAZ of the AA8011 side in all the passes was found to be lower compared to the stir zone. The stir zone hardness was found to be higher compared to the base material AA8011 hardness. Additionally, looking at the hardness of the stir zone to the AA8011 base material of the 3-pass SFSP for the specimen extracted towards the end of the joint, it can be seen that it was notably lower due to the defects on the position as a result of being cut too close to the SFSP tool exit hole. This is due to the submerged conditions preventing the material softening and coarsening of the grains [17,23–25]. The 1-pass hardness of the stir zone maximum hardness was found to be 75 HV, 65 HV for the 2-pass, 65 HV for the 3-pass and 67 HV for the 4-pass specimen.

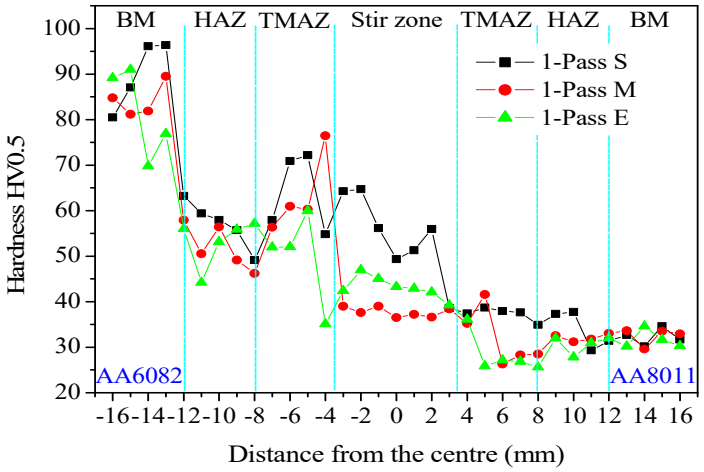

(**a**)

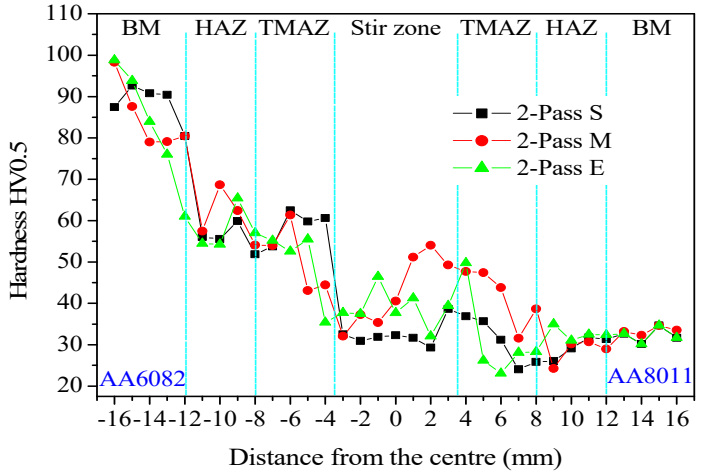

(**b**)

Figure 8. *Cont.*

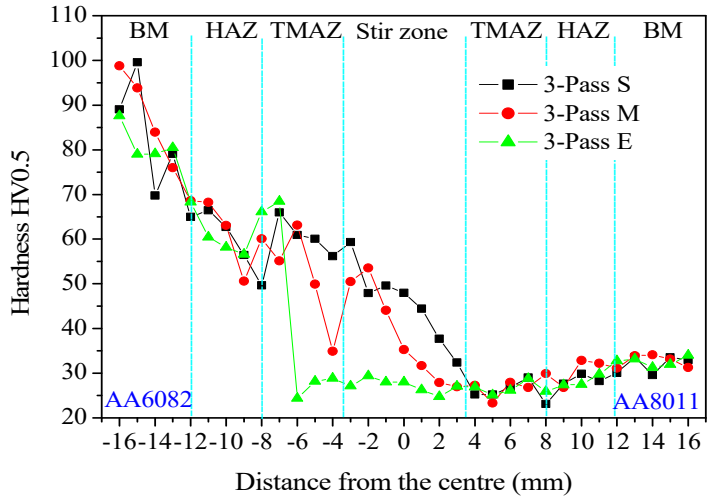

(**c**)

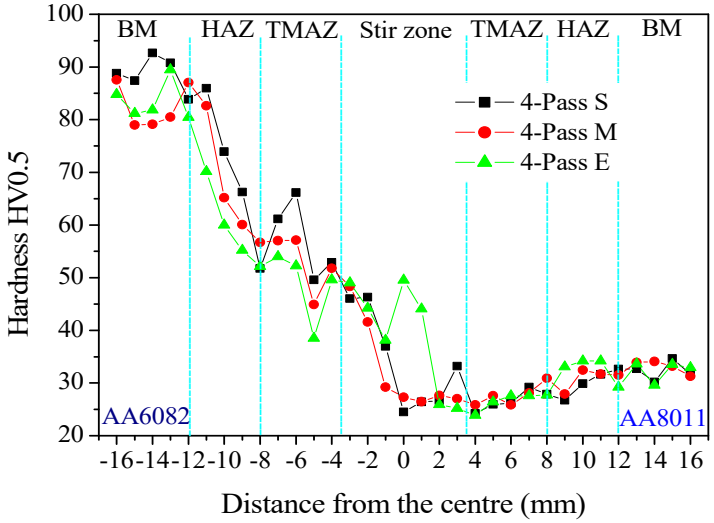

(**d**)

Figure 8. SFSP Hardness profiles, (**a**) 1-pass, (**b**) 2-pass, (**c**) 3-pass and (**d**) 4-pass.

4. Conclusions

The effects of multiple passes of the submerged friction stir-processed friction stir-welded AA6082-AA8011 dissimilar joints on the microstructure and mechanical properties were successfully investigated. Based on the results obtained, the following conclusions can be drawn:

1. There was no particular trend in the microstructure and mechanical positioning when looking at the specimen positioning in all the passes. The mean grain sizes were refined from 15.12 to 5.42 μm. The minimum mean grain sizes were refined from 3.54 to 1.49 μm and the standard deviation from 5.43 to 1.87 μm.
2. The ultimate tensile strength was improved from 84.96 to 94.77 MPa. The four-pass SFSPed specimens were found to have more ductile properties compared to the one-pass SFSPed specimen. The percentage elongation of the joints was improved from 18.13% to 24.13%. The fracture surface morphologies revealed a ductile failure mode.
3. The hardness of the stir zones in all the passes was found to be higher compared to the AA8011 base material but lower than the AA6082 one. The maximum stir zone hardness of 75 HV was observed on the one-pass SFSP joints.

Author Contributions: Conceptualization and validation, V.M. and S.M.; methodology, formal analysis, investigation, data curation, writing—original draft preparation, writing—review and editing and visualization, S.M.; software, resources, project administration, supervision and funding acquisition, V.M.; Both authors have read and agreed to the published version of the manuscript.

Funding: This research was funded by National Research Foundation Thuthuka Grant, grant number 118046 and the APC was funded by Cape Peninsula University of Technology.

Acknowledgments: The authors would like to acknowledge the Cape Peninsula University of Technology mechanical engineering workshop staff, and especially S. Petersen for her assistance in specimen preparation. Special appreciation also goes to Miranda Waldron from the University of Cape Town for assistance with scanning electron microscopy tests.

Conflicts of Interest: The authors declare no conflict of interest.

References

1. Barmouz, M.; Zall, V.; Pashazadeh, H. Mechanical and Microstructural Characterization of Hybrid Cu-SiC-Zn Composites Fabricated Via Friction Stir Processing. *Mater. Res.* **2016**, *19*, 1292–1298. [CrossRef]
2. Mishra, R.; Ma, Z. Friction stir welding and processing. *Mater. Sci. Eng. R Rep.* **2005**, *50*, 1–78. [CrossRef]
3. Peng, J.; Zhang, Z.; Liu, Z.; Li, Y.; Guo, P.; Zhou, W.; Wu, Y. The effect of texture and grain size on improving the mechanical properties of Mg-Al-Zn alloys by friction stir processing. *Sci. Rep.* **2018**, *8*, 1–9. [CrossRef]
4. Mabuwa, S.; Msomi, V. Effect of Friction Stir Processing on Gas Tungsten Arc-Welded and Friction Stir-Welded 5083-H111 Aluminium Alloy Joints. *Adv. Mater. Sci. Eng.* **2019**, *2019*, 3510236. [CrossRef]
5. Narayana, Y.; Sivanandam, A.; Sharma, V. Fabrication of Al5083/B4C surface composite by friction stir processing and its tribological characterization. *J. Mater. Res. Technol.* **2015**, *4*, 398–410.
6. Orozco-Caballero, A.; Ruano, O.A.; Rauch, E.F.; Carreño, F. Severe friction stir processing of an Al-Zn-Mg-Cu alloy: Misorientation and its influence on superplasticity. *Mater. Des.* **2018**, *137*, 128–139. [CrossRef]
7. Ma, Z.; Mishra, R.S.; Mahoney, M.; Grimes, R. High strain rate superplasticity in friction stir processed Al–Mg–Zr alloy. *Mater. Sci. Eng. A* **2003**, *351*, 148–153. [CrossRef]
8. Mohan, A.; Yuan, W.; Mishra, R.S. High strain rate superplasticity in friction stir processed ultrafine grained Mg-Al-Zn alloys. *Mater. Sci. Eng. USA* **2013**, *562*, 69–76. [CrossRef]
9. Sharma, V.; Singla, Y.K.; Gupta, Y.; Raghuwanshi, J. Post-processing of metal matrix composites by friction stir processing. *AIP Conf. Proc.* **1953**, *2018*, 090062.
10. Das, H.; Mondal, M.; Hong, S.-T.; Chun, D.-M.; Han, H. Joining and fabrication of metal matrix composites by friction stir welding/processing. *Int. J. Precis. Eng. Manuf. Technol.* **2018**, *5*, 151–172. [CrossRef]
11. Kurtyka, P.; Rylko, N.; Tokarski, T.; Wójcicka, A.; Pietras, A. Cast aluminium matrix composites modified with using FSP process—Changing of the structure and mechanical properties. *Compos. Struct.* **2015**, *133*, 959–967. [CrossRef]
12. Reddy, G.M.; Rao, K.S. Enhancement of wear and corrosion resistance of cast A356 aluminium alloy using friction stir processing. *Trans. Indian Inst. Met.* **2010**, *63*, 793–798. [CrossRef]
13. Darras, B.M.; Kishta, E.E. Submerged friction stir processing of AZ31 Magnesium alloy. *Mater. Des.* **2013**, *47*, 133–137. [CrossRef]
14. Chai, F.; Zhang, D.; Li, Y.; Zhang, W. High strain rate superplasticity of a fine-grained AZ91 magnesium alloy prepared by submerged friction stir processing. *Mater. Sci. Eng. A* **2013**, *568*, 40–48. [CrossRef]
15. Liu, H.J.; Feng, X.L. Effect of post-processing heat treatment on microstructure and microhardness of water-submerged friction stir processed 2219-T6 aluminum alloy. *Mater. Des.* **2013**, *47*, 101–105. [CrossRef]
16. Feng, X.; Liu, H.; Lippold, J.C. Microstructure characterization of the stir zone of submerged friction stir processed aluminum alloy 2219. *Mater. Charact.* **2013**, *82*, 97–102. [CrossRef]
17. Mabuwa, S.; Msomi, V. The impact of submerged friction stir processing on the friction stir welded dissimilar joints. *Mater. Res. Express* **2020**, *7*, 096513. [CrossRef]
18. Patel, V.; Badheka, V.; Li, W.; Akkireddy, S. Hybrid friction stir processing with active cooling approach to enhance superplastic behavior of AA7075 aluminum alloy. *Arch. Civ. Mech. Eng.* **2019**, *19*, 1368–1380. [CrossRef]
19. Rathinasuriyan, C.; Senthil, V.S. Modelling and optimization of submerged friction stir welding parameters for AA6061-T6 alloy using RSM. *Met. Mater.* **2016**, *54*, 297–304. [CrossRef]

20. Wang, J.; Lu, Y.; Zhou, D.; Zhang, Y.; Bai, Z.; Li, X. Effects of cooling condition on microstructural evolution and mechanical properties of friction stir processed 2A14 aluminum alloy. *Mater. Res. Express* **2019**, *6*, 126577. [CrossRef]
21. Chai, F.; Zhang, D.; Li, Y. Microstructures and tensile properties of submerged friction stir processed AZ91 magnesium alloy. *J. Magnes. Alloy.* **2015**, *3*, 203–209. [CrossRef]
22. Huang, G.; Yan, Y.; Wu, J.; Shen, Y.; Gerlich, A. Microstructure and mechanical properties of fine-grained aluminum matrix composite reinforced with nitinol shape memory alloy particulates produced by underwater friction stir processing. *J. Alloys Compd.* **2019**, *786*, 257–271. [CrossRef]
23. Srivastava, M.; Rathee, S.; Maheshwari, S.; Siddiquee, A.N. Influence of multiple-passes on microstructure and mechanical properties of Al-Mg/SiC surface composites fabricated via underwater friction stir processing. *Mater. Res. Express* **2018**, *5*, 066511. [CrossRef]
24. Huang, G.; Wu, J.; Hou, W.; Shen, Y. Microstructure, mechanical properties and strengthening mechanism of titanium particle reinforced aluminum matrix composites produced by submerged friction stir processing. *Mater. Sci. Eng. USA* **2018**, *734*, 353–363. [CrossRef]
25. Satyanarayana, M.; Kumar, A. Effect of heat treatment on AA2014 alloy processed through multi-pass friction stir processing. *J. Phys. Conf. Ser.* **2019**, *1240*, 012077. [CrossRef]
26. Zhang, Q.; Xiao, B.; Wang, Q.; Ma, Z. In situ Al_3Ti and Al_2O_3 nanoparticles reinforced Al composites produced by friction stir processing in an Al-TiO_2 system. *Mater. Lett.* **2011**, *65*, 2070–2072. [CrossRef]
27. Sharifitabar, M.; Sarani, A.; Khorshahian, S.; Afarani, M.S. Fabrication of 5052Al/Al_2O_3 nanoceramic particle reinforced composite via friction stir processing route. *Mater. Des.* **2011**, *32*, 4164–4172. [CrossRef]
28. Selvaraj, G.; Karthikeyan, T.; Mohanadass, R.; Indhumath, S. Investigation on mechanical properties of welded aluminium joints of aa 8011 using friction stir welding. *Int. J. Appl. Eng. Res.* **2015**, *10*, 11095–11100.
29. Kumar, H.M.A.; Ramana, V.V.; Pawar, M. Experimental Study on Dissimilar Friction Stir welding of Aluminium Alloys (5083-H111 and 6082-T6) to investigate the mechanical properties. *IOP Conf. Ser. Mater. Sci. Eng. USA* **2018**, *330*, 012076. [CrossRef]
30. Mabuwa, S.; Msomi, V. Comparative analysis between normal and submerged friction stir processed friction stir welded dissimilar aluminium alloy joints. *J. Mater. Res. Technol.* **2020**, *9*, 9632–9644. [CrossRef]
31. Eyvazian, A.; Hamouda, A.; Tarlochan, F.; Derazkola, H.A.; Khodabakhshi, F. Simulation and experimental study of underwater dissimilar friction-stir welding between aluminium and steel. *J. Mater. Res. Technol.* **2020**, *9*, 3767–3781. [CrossRef]
32. Khodabakhshi, F.; Gerlich, A.; Simchi, A.; Kokabi, A. Cryogenic friction-stir processing of ultrafine-grained Al–Mg–TiO_2 nanocomposites. *Mater. Sci. Eng. USA* **2015**, *620*, 471–482. [CrossRef]
33. Khodabakhshi, F.; Nosko, M.; Gerlich, A. Dynamic restoration and crystallographic texture of a friction-stir processed Al–Mg–SiC surface nanocomposite. *Mater. Sci. Technol.* **2018**, *34*, 1773–1791. [CrossRef]
34. Luo, X.C.; Zhang, D.T.; Cao, G.H.; Qiu, C.; Chen, D.L. Multi-pass submerged friction stir processing of AZ61 magnesium alloy: Strengthening mechanisms and fracture behavior. *J. Mater. Sci.* **2019**, *54*, 8640–8654. [CrossRef]
35. Chandrana, R.; Santhanam, S.K.V. Submerged friction stir welding of 6061-T6 aluminium alloy under different water heads. *Mater. Res.* **2018**, *21*, 1–12. [CrossRef]
36. Luo, X.; Zhang, D.; Zhang, W.; Qiu, C.; Chen, D. Tensile properties of AZ61 magnesium alloy produced by multi-pass friction stir processing: Effect of sample orientation. *Mater. Sci. Eng. USA* **2018**, *725*, 398–405. [CrossRef]
37. Ramesh, K.N.; Pradeep, S.; Pancholi, V. Multipass friction-stir processing and its effect on mechanical properties of aluminum alloy 5086. *Metall. Mater. Trans. A* **2012**, *43*, 4311–4319. [CrossRef]
38. Cavaliere, P.; Squillace, A.; Panella, F.W. Effect of welding parameters on mechanical and microstructural properties of AA6082 joints produced by friction stir welding. *J. Mater. Process. Technol.* **2008**, *200*, 364–372. [CrossRef]
39. Kumar, S.R.; Rao, V.S.; Pranesh, R. Effect of Welding Parameters on Macro and Microstructure of Friction Stir Welded Dissimilar Butt Joints between AA7075-T651 and AA6061-T651 Alloys. *Procedia Mater. Sci.* **2014**, *5*, 1726–1735. [CrossRef]
40. Sanaty-Zadeh, A. Comparison between current models for the strength of particulate-reinforced metal matrix nanocomposites with emphasis on consideration of Hall–Petch effect. *Mater. Sci. Eng. USA* **2012**, *531*, 112–118. [CrossRef]

41. Barcellona, A.; Buffa, G.; Fratini, L.; Palmeri, D. On microstructural phenomena occurring in friction stir welding of aluminium alloys. *J. Mater. Process. Technol.* **2006**, *177*, 340–343. [CrossRef]
42. Sameer; Birru, A.K. Mechanical and metallurgical properties of friction stir welded dissimilar joints of AZ91 magnesium alloy and AA 6082-T6 aluminium alloy. *J. Magnes. Alloy.* **2019**, *7*, 264–271. [CrossRef]
43. Niu, P.; Li, W.Y.; Chen, D. Strain hardening behavior and mechanisms of friction stir welded dissimilar joints of aluminum alloys. *Mater. Lett.* **2018**, *231*, 68–71. [CrossRef]

Publisher's Note: MDPI stays neutral with regard to jurisdictional claims in published maps and institutional affiliations.

© 2020 by the authors. Licensee MDPI, Basel, Switzerland. This article is an open access article distributed under the terms and conditions of the Creative Commons Attribution (CC BY) license (http://creativecommons.org/licenses/by/4.0/).